Vol 464|15 April 2010|doi:10.1038/nature08978

LETTERS

Migrastatin analogues target fascin to block tumour metastasis

Lin Chen[1]*, Shengyu Yang[1]*, Jean Jakoncic[2], J. Jillian Zhang[1] & Xin-Yun Huang[1]

Tumour metastasis is the primary cause of death of cancer patients. Development of new therapeutics preventing tumour metastasis is urgently needed. Migrastatin is a natural product secreted by *Streptomyces*[1,2], and synthesized migrastatin analogues such as macroketone are potent inhibitors of metastatic tumour cell migration, invasion and metastasis[3–6]. Here we show that these migrastatin analogues target the actin-bundling protein fascin to inhibit its activity. X-ray crystal structural studies reveal that migrastatin analogues bind to one of the actin-binding sites on fascin. Our data demonstrate that actin cytoskeletal proteins such as fascin can be explored as new molecular targets for cancer treatment, in a similar manner to the microtubule protein tubulin.

To understand the molecular basis by which migrastatin analogues inhibit tumour cell migration and tumour metastasis, we pursued the biochemical identification of the protein target for macroketone. We took an affinity protein purification approach using synthesized biotin-labelled macroketone[4] (Fig. 1a). Biotin-conjugated macroketone inhibited 4T1 breast tumour cell migration with a similar potency (50% inhibitory concentration (IC_{50}) $\approx$ 300 nM) to that of the non-biotinylated macroketone ($IC_{50} \approx 100$ nM)[4]. 4T1 tumour cell extracts were incubated with biotin-conjugated macroketone or with free biotin. Strepavidin-conjugated agarose beads were added. After extensive washes, bound proteins were eluted and resolved by SDS–PAGE. A protein of about 58 kDa was specifically detected in the sample from affinity-purified proteins with biotin-conjugated macroketone, but not in the sample with free biotin (Fig. 1b). This roughly 58-kDa protein was identified by mass spectrometry and by peptide sequence as mouse fascin 1. Fascin is the primary actin cross-linker in filopodia and is required to crosslink the actin filaments maximally into straight, compact, rigid bundles[7–12]. Elevated expressions of fascin messenger RNA and protein in cancer cells have been correlated with an aggressive clinical course, poor prognosis and shorter survival[13–21].

Next we verified that macroketone does indeed interact directly with fascin. We purified recombinant glutathione *S*-transferase (GST)-tagged fascin to homogeneity from *Escherichia coli* (Supplementary Fig. 1a). Purified fascin, but not GST control, interacted specifically with biotin-conjugated macroketone (Fig. 1c). Moreover, an excess of non-biotinylated macroketone efficiently competed with the binding between fascin and biotin-conjugated macroketone (Supplementary Fig. 1b). Another migrastatin analogue, macrolactam, also competed with biotin-conjugated macroketone for binding to fascin. Taken together, these data demonstrate that fascin is a protein target of macroketone.

We then examined the biochemical effect of macroketone on the activity of fascin. We have used three different approaches to investigate the effect. First, we used purified recombinant fascin protein and investigated its actin-bundling activity with the F-actin pelleting assay[9]. In this low-speed centrifugation assay, the pellets contain bundles of F-actin polymers[9]. Purified fascin increased the amounts of F-actin bundles in the pellets (Fig. 1d, e). Although macroketone alone had no effect on the formation of F-actin bundles, macroketone significantly decreased the fascin-induced bundling of F-actin polymers (Fig. 1d, e). Second, we used fluorescence microscopy to reveal the fascin-regulated F-actin filament bundles in the absence and presence of macroketone (Supplementary Fig. 2a, b). The addition of fascin induced the formation of F-actin bundles, as revealed by the staining of F-actin filaments with rhodamine-conjugated phalloidin (Supplementary Fig. 2a). In contrast, in the presence of macroketone, the formation of F-actin bundles was largely (more than 80%) inhibited (Supplementary Fig. 2a, b). Third, we used electron microscopy to examine the actin bundles (Fig. 1f and Supplementary Fig. 2c). This examination revealed that macroketone decreased the thickness of the bundles. These data demonstrate that macroketone inhibits the actin-bundling activity of fascin.

To reveal the structural basis for the inhibition of fascin function by migrastatin analogues, we solved the X-ray crystal structures of fascin in the absence and presence of a migrastatin analogue (Fig. 2). We determined the native fascin structure and the structure of the fascin–macroketone complex at 1.8 Å and 2.7 Å, respectively (Fig. 2 and Supplementary Table 1). The overall structure of fascin has four β-trefoil folds, with each β-trefoil comprising six two-stranded β-hairpins (Fig. 2a–c, Supplementary Figs 3–5 and Supplementary Tables 2–4). This structure is similar to one fascin structure deposited in the protein structural database (Supplementary Fig. 6). The overall domain arrangement of the fascin–macroketone complex is very similar to that of the native fascin (Fig. 2d). The bound macroketone molecule sits at the surface of trefoil 4, on the side facing the cleft between trefoils 4 and 1 (Fig. 2d, e and Supplementary Fig. 7). Macroketone is held in place by interaction with the side chains of His 392, Glu 391, Ala 488, Lys 471 and His 474 as well as the α carbon of Asp 473 (Fig. 2d, e and Supplementary Fig. 8). His 392 and His 474 contribute to the binding of macroketone through hydrogen bonds (Fig. 2e). The interaction between fascin and macroketone is further stabilized by the van der Waals force between the macrolide ring carbon and residues Glu 391, Ala 488, Lys 471 and Asp 473 (Fig. 2e). These structural data are consistent with our previous structure–activity studies on migrastatin analogues showing that the macrolide ring, instead of the lengthy side chain of migrastatin, was important for the inhibitory function on tumour cell migration[4].

The structure of the fascin–macroketone complex immediately suggests a possible biochemical mechanism by which macroketone inhibits the actin-bundling activity of fascin. The macroketone binding site is one of the actin-binding sites on fascin (Fig. 3a). We therefore propose that macroketone binding interferes with the binding of actin filament to fascin. Fascin functions as a monomer to

[1]Department of Physiology, Cornell University Weill Medical College, New York, New York 10065, USA. [2]Brookhaven National Laboratory, National Synchrotron Light Source, Upton, New York 11973, USA.
*These authors contributed equally to this work.

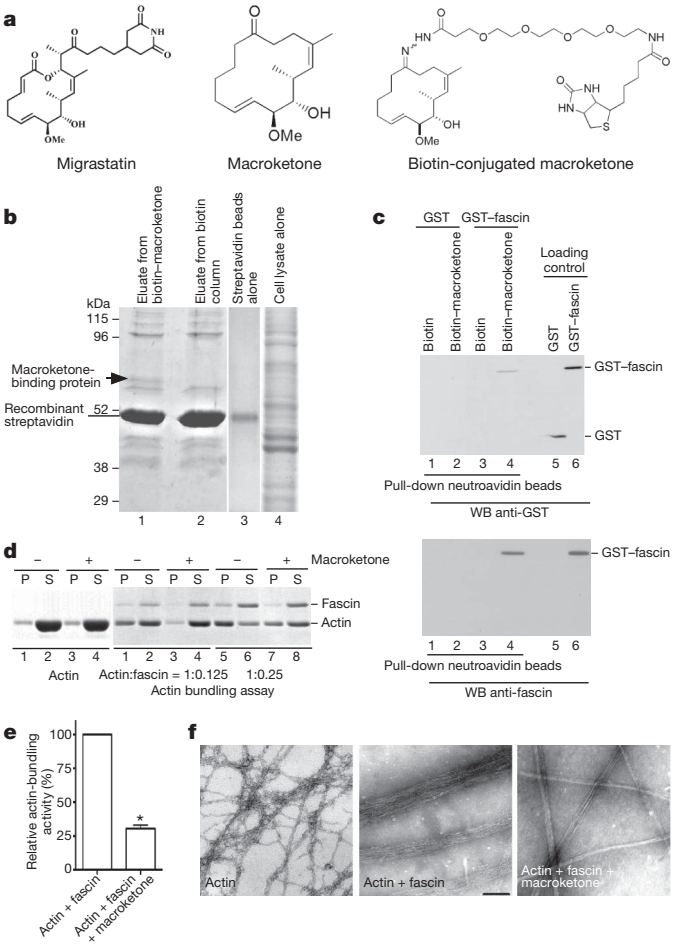

Figure 1 | Identification of fascin as a macroketone target. **a**, Diagram of the structures of migrastatin, one of its analogues (the macroketone core) and the biotin-conjugated macroketone core. **b**, Coomassie blue stain of the SDS–PAGE gel after protein affinity purification. The arrow indicates the band identified as mouse fascin 1. **c**, Direct interaction of fascin with macroketone. Neutroavidin-agarose beads with biotin-conjugated macroketone (10 μM) or biotin (10 μM) were mixed with GST–fascin or GST. WB, western blot. Data are representative of three experiments with similar results. **d**, Assay of the actin-bundling activity with a low-speed co-sedimentation assay. Polymerized F-actin (1 μM) was incubated with 0.125 μM or 0.25 μM purified fascin in the presence or absence of macroketone (10 μM). Supernatants (S) or pellets (P) were analysed by SDS–PAGE followed by Coomassie blue staining. The result shown is representative of five experiments with similar outcomes. **e**, Quantification of F-actin bundling assays from **d**. Results are means and s.d. ($n = 5$; asterisk, $P < 0.05$). **f**, Electron microscopy of fascin-induced F-actin bundles in the presence or absence of macroketone. F-actin (1 μM) was incubated with fascin (0.125 μM) in the presence or absence of macroketone (10 μM). Representative images are shown. Scale bar, 50 nm.

bundle actin filaments, and it has been proposed that fascin has two actin-binding sites for this bundling activity[22]. Previous mutagenesis studies implied that both the amino and carboxy termini of fascin contribute to actin binding. Our crystal structure implicates that the N and C termini constitute one of the actin-binding sites (Fig. 3a). Both the N and C termini are located in the same cleft (Fig. 3a). Furthermore, a stretch of residues (29–42) at the N terminus, which has similarity to an actin-binding site of MARCKS (myristoylated alanine-rich C-kinase substrate)[23], is also facing the trefoil 1–4 cleft (Fig. 3a). Moreover, the actin-bundling activity of fascin is negatively regulated by a protein kinase C phosphorylation site (Ser 39) within the N-terminal region[22] (Fig. 3a). Taken together, these data suggest that this cleft is one of the actin-binding sites.

To investigate this hypothesis that the macroketone-binding site overlaps with one of the actin-binding sites, we mutated five residues

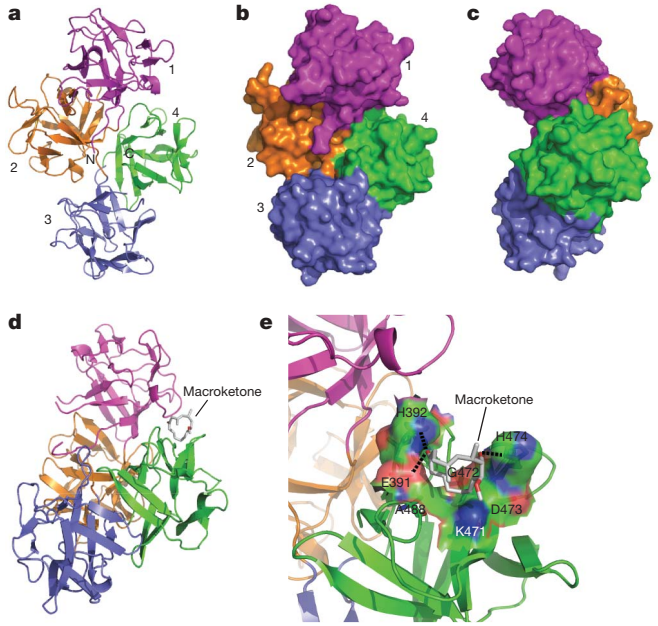

Figure 2 | X-ray crystal structures of fascin and of the complex of fascin and macroketone. **a**, Structure of fascin shown as a ribbon diagram, viewed from the N-terminal and C-terminal plane. The four β-trefoil domains are coloured magenta (trefoil 1), orange (trefoil 2), blue (trefoil 3) and green (trefoil 4). **b**, Surface presentation of fascin structure viewed in **a**. **c**, View of fascin turned clockwise 90° along the *y* axis relative to the view in **b**. **d**, Overall structure of the complex of fascin and macroketone. The macroketone molecule is shown as a white stick model. **e**, Macroketone-binding site. Residues involved in interactions with macroketone are shown as surface, and hydrogen bonds are shown as dashed lines.

involved in macroketone binding and examined the actin-bundling activity of those fascin mutants (Fig. 3b–d). We found that mutations of His 392, Lys 471 and Ala 488 did indeed decrease the actin-bundling activity of fascin (Fig. 3c, d). These data show that residues involved in macroketone binding are involved in actin bundling. We also examined the sensitivity of the actin-bundling activity of Glu 391 and His 474 to macroketone (mutants His 392, Lys 471 and Ala 488 were not tested because of their defective actin-bundling activity). As shown in Fig. 3e, f, mutation of His 474 to Ala rendered fascin resistant to macroketone treatment. Moreover, this His 474 to Ala mutant fascin did not bind to biotin–macroketone (Fig. 3g). Taken together, our data demonstrate that several fascin residues (such as His 392, Lys 471 and Ala 488) involved in macroketone binding also contribute to actin binding. Hence, the macroketone binding site is one of the actin-binding sites.

To critically evaluate further the possibility that macroketone inhibits fascin to decrease tumour cell migration, invasion and metastasis, it would be best to have a fascin mutant that does not bind to macroketone but retains its actin-bundling activity. This mutant fascin should confer resistance to macroketone in tumour cell migration, invasion and metastasis. Our data above showed that His 474 is essential for macroketone binding but not for actin bundling (Fig. 3). To confirm that the fascin His474Ala mutant could support tumour cell migration, invasion and metastasis, we used RNA interference to downregulate fascin protein levels in 4T1 mouse mammary tumour cells. Whereas two fascin short hairpin RNAs (shRNAs) knocked down the fascin protein levels, a control shRNA did not (Supplementary Fig. 9a). Fascin shRNA-treated cells grew at rates comparable to those of control shRNA-treated cells and non-transfected 4T1 cells in full growth medium (Supplementary Fig. 9b), suggesting that fascin is not required for the proliferation of breast tumour cells *in vitro*. This is consistent with our previous observation that migrastatin analogues had no effect on tumour cell proliferation and primary tumour growth in mouse models[5]. A Boyden-chamber cell migration

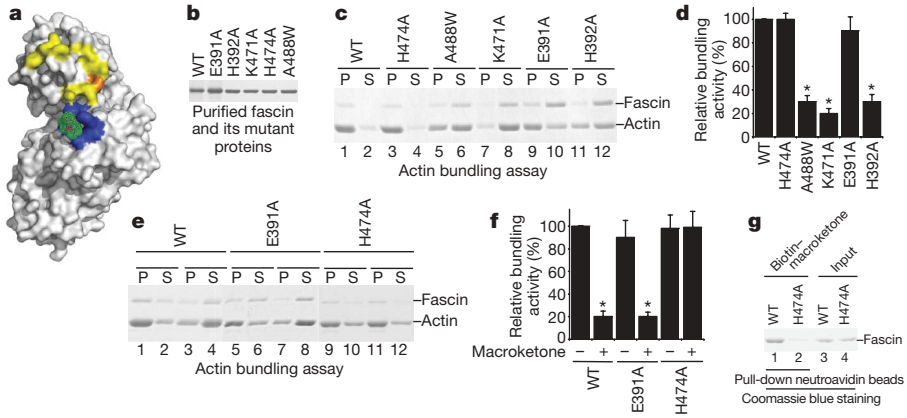

Figure 3 | Macroketone-binding site overlaps with one of the actin-binding sites. **a**, Surface presentation of the structure of the complex of fascin and macroketone. Residues involved in macroketone binding are shown in blue. Sequences (residues 29–42) homologous to the MARCKS actin-binding site are coloured yellow, and the protein kinase C phosphorylation site (Ser 39) is coloured orange. Macroketone is shown as a green mesh. **b**, Coomassie blue stain of purified fascin and its mutant proteins. WT, wild type. **c**, Actin bundling assay for the wild-type fascin and its mutants. P, pellet; S, supernatant. **d**, Quantification of data in **c**. Results are means and s.d. ($n = 3$, $P < 0.05$). **e**, Sensitivity to macroketone. Wild-type fascin and the E391A and H474A mutants of fascin were assayed for their actin-bundling activity in the absence or presence of macroketone (10 μM). **f**, Quantification of data in **e**. Results are means and s.d. ($n = 3$, $P < 0.05$). **g**, H474A fascin mutant protein fails to bind biotin–macroketone. The residual H474A protein pulled down by biotin–macroketone (lane 2) was aggregates bound to the beads.

assay showed that treatment with fascin shRNA, but not with the control shRNA, decreased the serum-induced migration of 4T1 cells (Supplementary Fig. 9c). Moreover, this inhibitory effect of fascin shRNA could be rescued by transfection of human fascin cDNA (there are two nucleotide changes without amino-acid changes in this specific region) (Fig. 4a). This rescued migration was sensitive to macroketone (Fig. 4a). Although mutations of His 474 to either Lys (*Drosophila* fascin has a Lys in the corresponding position) or Ala in human fascin also rescued the migration of 4T1 cells treated with fascin siRNAs (Fig. 4a), these rescued migrations were not inhibited by macroketone (Fig. 4a and Supplementary Fig. 9d). In addition, we performed rescue experiments of fascin shRNA-treated 4T1 cells with villin, another actin-bundling protein. From *Drosophila* genetic studies, villin partly rescued the phenotypes of fascin mutations during *Drosophila* oogenesis[24]. Villin did not bind macroketone *in vitro*, and overexpression of villin in fascin shRNA-treated 4T1 cells partly rescued the migration, which was insensitive to macroketone (Supplementary Fig. 9e). Similarly, expression of human wild-type fascin and the His474Ala fascin mutant in fascin shRNA-treated mouse 4T1 cells rescued tumour cell invasion (Fig. 4b). The rescued invasion by wild-type fascin but not by His474Ala mutant fascin was sensitive to macroketone (Fig. 4b and Supplementary Fig. 9f). Moreover, fascin

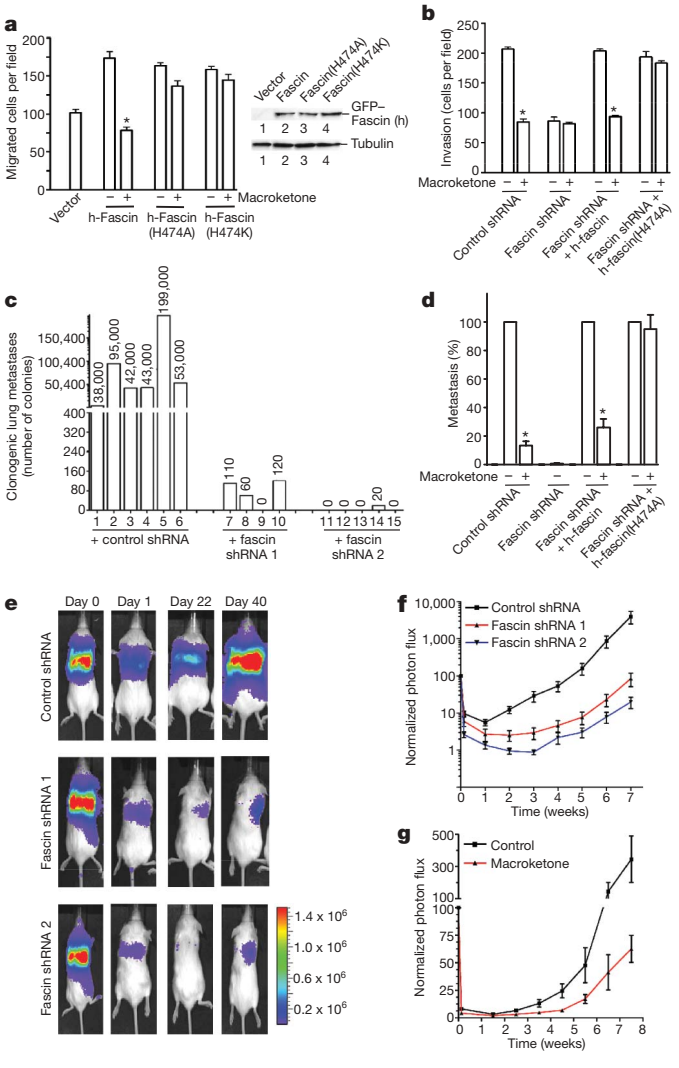

Figure 4 | Fascin His 474 mutation renders tumour cell migration, invasion and metastasis resistant to macroketone. **a**, Left: Boyden-chamber cell migration assay of mouse fascin shRNA 2-treated 4T1 cells transfected with various mutants of GFP–human fascin (h-fascin) in the presence or absence of macroketone (10 μM). Right: overexpression of various fascin mutants in mouse fascin shRNA-2-treated 4T1 cells. Results are means and s.d. ($n = 5$, $P < 0.05$). **b**, *In vitro* Matrigel invasion assay with mouse fascin shRNA-treated 4T1 cells overexpressing wild-type human fascin or fascin(H474A) mutant in the presence or absence of macroketone (10 μM). Results are means and s.d. ($n = 5$, $P < 0.05$). **c**, Total number of metastatic colonies in lungs of individual mice four weeks after injection of 4T1 cells expressing control shRNA and two fascin shRNAs. The numbers 1 to 15 on the *x* axis are mouse identification numbers. **d**, Tumour metastasis assay with mouse fascin shRNA-treated 4T1 cells overexpressing wild-type human fascin or fascin(H474A) mutant in the presence or absence of macroketone (10 mg kg^{-1}). Comparison of the fascin shRNA group with the control shRNA group. Results are means and s.d. ($n = 5$~6, $P < 0.05$). **e**, Representative non-invasive bioluminescence images of mice at the indicated times after injection of human MDA-MB-231 cells expressing control shRNA and two fascin shRNAs. **f**, Normalized photon flux of non-invasive bioluminescence images of mice at the indicated times after injection of human MDA-MB-231 cells expressing control shRNA and two fascin shRNAs. Results are means ± s.d. **g**, Normalized photon flux of non-invasive bioluminescence images of mice at the indicated times after injection of human MDA-MB-231 cells in the presence or absence of macroketone (10 mg kg^{-1}). Results are means ± s.d.

His474Ala mutation conferred macroketone resistance in tumour metastasis (Fig. 4c, d). Treatment with fascin shRNA abolished 4T1 tumour cell metastasis in mouse models (Fig. 4c, d). Macroketone significantly inhibited metastasis in mice injected with control shRNA-treated cells. Wild-type human fascin-rescued 4T1 cells metastasized to the lung, and this metastasis was inhibited by macroketone (Fig. 4d). In contrast, although re-expression of His474Ala mutant fascin rescued the tumour metastasis, this metastasis was insensitive to macroketone (Fig. 4d). These results further confirm that fascin is the protein target for macroketone in its inhibition of tumour cell migration, invasion and metastasis.

Mindful of the clinical potential of fascin inhibitors for human cancer treatments, we further investigated the inhibition of lung colonization of human breast tumour cells in immune-deficient mouse models by fascin inhibitors such as fascin shRNAs and macroketone. First, MDA-MB-231 cells were retrovirally infected with a triple-fusion protein reporter construct encoding herpes simplex virus thymidine kinase 1, green fluorescent protein (GFP) and firefly luciferase (TGL)[25,26]. These cells were injected into the tail vein of immunodeficient mice (NOD-SCID mice). The colonization of the lung by tumour cells was monitored by non-invasive bioluminescence imaging (Fig. 4e, f and Supplementary Fig. 10a–d)[20]. A substantial attenuation of the bioluminescence signal was observed within the first few days, indicating that cells that failed to metastasize were not able to survive (Fig. 4e, f). Progressively increasing signals after two weeks in mice with control shRNA-treated tumour cells indicated that cells had succeeded in metastasizing and proliferating (Fig. 4e, f). The presence of fascin shRNA-treated cells in the lung was much less than in control shRNA-treated cells (Fig. 4e, f). Fascin shRNA treatments therefore significantly inhibited the lung colonization. Second, we have also shown here that macroketone could effectively block the lung colonization of human breast tumours in an animal model. As shown in Fig. 4g, macroketone decreased the lung colonization of MDA-MB-231 cells by more than 80%. Taken together, our data demonstrate the feasibility of using the inhibitors of fascin (such as macroketone and the siRNAs) as therapeutic agents for treating metastatic breast tumours.

Fascin mRNA transcript and protein levels are significantly elevated in clinically aggressive tumours[17,27]. Overexpression of fascin leads to increases in cell migration and invasion[28,29]. We analysed a microarray gene expression data set with 137 breast cancer samples and 16 normal breast samples from patients treated at the Memorial Sloan-Kettering Cancer Center. Breast tumour samples showed increased fascin expression in comparison with normal samples. Moreover, we observed a high level of fascin transcripts in an oestrogen receptor (ER)-negative group of patients (Supplementary Fig. 11a) and a progesterone receptor (PR)-negative group of patients (Supplementary Fig. 11b). Immunohistology staining with an anti-fascin antibody confirmed that fascin protein was upregulated in ER-negative tumours (Supplementary Fig. 11c), whereas ER-positive tumour cells were negative for fascin staining (note that endothelia of vessels are fascin positive). We also analysed fascin mRNA expression levels in the Rosetta microarray data set of 295 breast cancer patients[30]. Similarly, we found that the levels of fascin transcripts were significantly higher in ER-negative and PR-negative tumours (Supplementary Fig. 11d, e).

Overexpression of fascin contributes to a more aggressive clinical course of cancer[16]. The Rosetta data set contains detailed clinical follow-up information on breast cancer patients. We therefore evaluated the clinical and pathological associations of fascin expression in breast cancer patients. Kaplan–Meier analyses showed that higher expression of fascin was associated with lower overall survival (Supplementary Fig. 11f) and lower metastasis-free survival (Supplementary Fig. 11g). These data highlight the correlation between higher fascin expression and metastasis and death in human breast cancer patients.

METHODS SUMMARY

Affinity purification. 4T1 tumour cells were lysed and the cell extract was then mixed with biotin-labelled macroketone or free biotin for 2 h at 4 °C with gentle rotation. Recombinant streptavidin-agarose beads (Pierce) were added to the cell extract and the incubation was continued for a further 2 h with gentle rotation. The mixtures were then loaded onto a Poly-Prep chromatography column. After extensive washing with cell lysis buffer, samples were eluted with elution buffer. The eluate was further concentrated with Centricon P-20 (Millipore) and separated by SDS–PAGE. The gel was stained with Coomassie blue and the indicated band was cut out for mass spectrometry and peptide sequencing analyses.

Breast tumour metastasis in mice. All animal work was performed in compliance with the Institutional Animal Care and Use Committee of Weill Medical College. Spontaneous 4T1 mouse breast tumour metastasis assay was performed as described previously[5,26]. In experimental lung metastasis experiments, NOD-SCID immunodeficient mice were used. MDA-MB-231 human breast tumour cells expressing the TGL reporter were trypsinized and washed with PBS. Subsequently 10^6 cells in 0.2 ml of PBS were injected into the lateral tail vein. Luciferase-based, non-invasive bioluminescent imaging and analysis were performed with an IVIS Imaging System (Xenogen).

Crystallization and structure determination. To obtain crystals of the fascin–macroketone complex, the protein was incubated for 1 h at room temperature (20–25 °C) in the protein buffer supplemented with 2 mM macroketone. Crystallization was performed at 20 °C with the vapour-diffusion hanging-drop method. Fascin crystallized in 100 mM HEPES pH 8.0, 16% PEG4000, 1% propan-2-ol. Both crystals (fascin without or with macroketone) belong to space group *C*2. X-ray diffraction data were recorded at National Synchrotron Light Source beamlines X6A and X4C at Brookhaven National Laboratory. A partial structure was initially solved by the MR-SAD method with a selenomethionine derivative sample that diffracted to 2.1 Å and a fraction of the 1DFC Protein Data Bank (PDB) file. This model was subsequently extended by iterative model building and refinement cycles with COOT and REFMAC5.

Full Methods and any associated references are available in the online version of the paper at www.nature.com/nature.

Received 24 September 2009; accepted 4 March 2010.

1. Nakae, K. *et al.* Migrastatin, a novel 14-membered lactone from *Streptomyces* sp. MK929–43F1. *J. Antibiot. (Tokyo)* **53,** 1228–1230 (2000).
2. Woo, E. J. *et al.* Migrastatin and a new compound, isomigrastatin, from *Streptomyces platensis*. *J. Antibiot. (Tokyo)* **55,** 141–146 (2002).
3. Njardarson, J. T., Gaul, C., Shan, D., Huang, X. Y. & Danishefsky, S. J. Discovery of potent cell migration inhibitors through total synthesis: lessons from structure–activity studies of (+)-migrastatin. *J. Am. Chem. Soc.* **126,** 1038–1040 (2004).
4. Gaul, C. *et al.* The migrastatin family: discovery of potent cell migration inhibitors by chemical synthesis. *J. Am. Chem. Soc.* **126,** 11326–11337 (2004).
5. Shan, D. *et al.* Synthetic analogues of migrastatin that inhibit mammary tumor metastasis in mice. *Proc. Natl Acad. Sci. USA* **102,** 3772–3776 (2005).
6. Ju, J. *et al.* Evaluation of new migrastatin and dorrigocin congeners unveils cell migration inhibitors with dramatically improved potency. *Bioorg. Med. Chem. Lett.* **18,** 5951–5954 (2008).
7. Otto, J. J., Kane, R. E. & Bryan, J. Formation of filopodia in coelomocytes: localization of fascin, a 58,000 dalton actin cross-linking protein. *Cell* **17,** 285–293 (1979).
8. Bryan, J. & Kane, R. E. Separation and interaction of the major components of sea urchin actin gel. *J. Mol. Biol.* **125,** 207–224 (1978).
9. Yamashiro-Matsumura, S. & Matsumura, F. Purification and characterization of an F-actin-bundling 55-kilodalton protein from HeLa cells. *J. Biol. Chem.* **260,** 5087–5097 (1985).
10. Vignjevic, D. *et al.* Formation of filopodia-like bundles *in vitro* from a dendritic network. *J. Cell Biol.* **160,** 951–962 (2003).
11. Vignjevic, D. *et al.* Role of fascin in filopodial protrusion. *J. Cell Biol.* **174,** 863–875 (2006).
12. Adams, J. C. Roles of fascin in cell adhesion and motility. *Curr. Opin. Cell Biol.* **16,** 590–596 (2004).
13. Maitra, A. *et al.* Immunohistochemical validation of a novel epithelial and a novel stromal marker of pancreatic ductal adenocarcinoma identified by global expression microarrays: sea urchin fascin homolog and heat shock protein 47. *Am. J. Clin. Pathol.* **118,** 52–59 (2002).
14. Pelosi, G. *et al.* Independent value of fascin immunoreactivity for predicting lymph node metastases in typical and atypical pulmonary carcinoids. *Lung Cancer* **42,** 203–213 (2003).
15. Hashimoto, Y., Shimada, Y., Kawamura, J., Yamasaki, S. & Imamura, M. The prognostic relevance of fascin expression in human gastric carcinoma. *Oncology* **67,** 262–270 (2004).
16. Hashimoto, Y., Skacel, M. & Adams, J. C. Roles of fascin in human carcinoma motility and signaling: prospects for a novel biomarker? *Int. J. Biochem. Cell Biol.* **37,** 1787–1804 (2005).

17. Yoder, B. J. *et al.* The expression of fascin, an actin-bundling motility protein, correlates with hormone receptor-negative breast cancer and a more aggressive clinical course. *Clin. Cancer Res.* **11,** 186–192 (2005).
18. Zigeuner, R., Droschl, N., Tauber, V., Rehak, P. & Langner, C. Biologic significance of fascin expression in clear cell renal cell carcinoma: systematic analysis of primary and metastatic tumor tissues using a tissue microarray technique. *Urology* **68,** 518–522 (2006).
19. Rodriguez-Pinilla, S. M. *et al.* Prognostic significance of basal-like phenotype and fascin expression in node-negative invasive breast carcinomas. *Clin. Cancer Res.* **12,** 1533–1539 (2006).
20. Minn, A. J. *et al.* Genes that mediate breast cancer metastasis to lung. *Nature* **436,** 518–524 (2005).
21. Wu, J. M. *et al.* Heterogeneity of breast cancer metastases: comparison of therapeutic target expression and promoter methylation between primary tumors and their multifocal metastases. *Clin. Cancer Res.* **14,** 1938–1946 (2008).
22. Ono, S. *et al.* Identification of an actin binding region and a protein kinase C phosphorylation site on human fascin. *J. Biol. Chem.* **272,** 2527–2533 (1997).
23. Mosialos, G. *et al.* Epstein–Barr virus infection induces expression in B lymphocytes of a novel gene encoding an evolutionarily conserved 55-kilodalton actin-bundling protein. *J. Virol.* **68,** 7320–7328 (1994).
24. Cant, K. & Cooley, L. Single amino acid mutations in *Drosophila* fascin disrupt actin bundling function *in vivo*. *Genetics* **143,** 249–258 (1996).
25. Minn, A. J. *et al.* Distinct organ-specific metastatic potential of individual breast cancer cells and primary tumors. *J. Clin. Invest.* **115,** 44–55 (2005).
26. Yang, S., Zhang, J. J. & Huang, X. Y. Orai1 and STIM1 are critical for breast tumor cell migration and metastasis. *Cancer Cell* **15,** 124–134 (2009).
27. Grothey, A., Hashizume, R., Sahin, A. A. & McCrea, P. D. Fascin, an actin-bundling protein associated with cell motility, is upregulated in hormone receptor negative breast cancer. *Br. J. Cancer* **83,** 870–873 (2000).
28. Hashimoto, Y., Parsons, M. & Adams, J. C. Dual actin-bundling and protein kinase C-binding activities of fascin regulate carcinoma cell migration downstream of Rac and contribute to metastasis. *Mol. Biol. Cell* **18,** 4591–4602 (2007).
29. Vignjevic, D. *et al.* Fascin, a novel target of β-catenin-TCF signaling, is expressed at the invasive front of human colon cancer. *Cancer Res.* **67,** 6844–6853 (2007).
30. van 't Veer, L. J. *et al.* Gene expression profiling predicts clinical outcome of breast cancer. *Nature* **415,** 530–536 (2002).

Supplementary Information is linked to the online version of the paper at www.nature.com/nature.

Acknowledgements J.J.Z. and X.Y.H. dedicate this paper to the memory of Yonghong Zhang, who died of cancer on 12 September 2009. We are grateful to W. Gerald (deceased) at Memorial Sloan-Kettering Cancer Center for letting us examine his DNA microarray data on human breast tumour samples for the fascin expression. We thank S. Almo for the fascin plasmid; S. Danishefsky and colleagues for the biotin-conjugated macroketone used in the initial exploration of the conditions for protein purification; members of the J. Massagué laboratory for teaching the use of the IVIS Imaging system; the personnel at the beamlines X6A and X4C of the National Synchrotron Light Source for the beamtime and for assistance; and D. Eliezer, T. Maack, L. Palmer, H. Wu and members of our laboratory for critically reading the manuscript. We thank S. Almo and his colleagues, H. Wu and J. Wu, for help with the crystallization experiments. This work was supported by grants from the National Institutes of Health (CA136837) and the Department of Defense (W81XWH-06-1-0362).

Author Contributions L.C., S.Y., J.J.Z. and X.Y.H. conceived the project. L.C. and S.Y. performed the experiments. S.Y. and J.J. determined the structures. L.C., S.Y., J.J.Z. and X.Y.H. analysed the data and wrote the paper.

Author Information The coordinates and structure factors of crystal structures of fascin and the fascin–macroketone complex have been deposited in the Protein Data Bank under accession numbers 3LLP and 3LNA, respectively. Reprints and permissions information is available at www.nature.com/reprints. The authors declare no competing financial interests. Correspondence and requests for materials should be addressed to X.Y.H. (xyhuang@med.cornell.edu).

METHODS

Materials. Mouse 4T1 mammary tumour cells and human MDA-MB-231 breast tumour cells were obtained from the American Type Culture Collection and have been described previously[31,32]. 4T1 cells were cultured in RPMI 1640 medium supplemented with 10% FBS. MDA-MB-231 cells were cultured in DMEM supplemented with 10% FBS. Macroketone and biotin-conjugated macroketone were custom synthesized by outside companies.

Affinity purification. 4T1 tumour cells were lysed in cell lysis buffer (50 mM Tris-HCl pH 7.4, 150 mM NaCl, 1% Nonidet P40, 0.1% SDS, and protease inhibitors: 1 mM phenylmethylsulphonyl fluoride, 10 μg ml^{-1} leupeptin, pepstatin and aprotinin). The cell extract was then mixed with biotin-labelled macroketone or free biotin for 2 h at 4 °C with gentle rotation. Streptavidin beads (Pierce) were added to the cell extract and the incubation was continued for a further 2 h with gentle rotation. The mixtures were then loaded onto the Poly-Prep chromatography column. After extensive washing with cell lysis buffer (with the NaCl concentration increased to 300 mM), samples were eluted three times with elution buffer (0.1 M glycine-HCl pH 2.8). The eluate was further concentrated with Centricon P-20 (Millipore) and separated by SDS–PAGE. The gel was stained with Coomassie blue and the indicated band was cut out for mass spectrometry and peptide sequencing analyses.

RNA interference. RNA-mediated interference of fascin was performed in 4T1 mouse breast tumour and MDA-MB-231 human breast tumour cells with pSUPER vector (Oligoengine). The target sequences of the two pairs of mouse fascin were 5′-GGTGGGCAAAGATGAGCTC-3′ and 5′-GTGGAGCGTGCA CATCGCC-3′. The target sequences of the two pairs of human fascin were 5′-GGTGGGCAAGGACGAGCTC-3′ and 5′-GCCTGAAGAAGAAGCAGAT-3′. Control shRNA was a shRNA that targets a LacZ sequence.

***In vitro* wound-healing assay.** Cell migration assays were performed as described previously[32,33]. Cells were allowed to form a confluent monolayer in a 24-well plate coated with gelatin, before being wounded. The wound was made by scraping a conventional pipette tip across the monolayer. Migration was induced by the addition of medium supplemented with 10% FBS. When the wound for the positive control had closed, cells were fixed with 3.7% formaldehyde and stained with crystal violet staining solution.

Boyden-chamber cell migration assay. Cells (5×10^4) suspended in starvation medium were added to the upper chamber of an insert (6.5 mm diameter, 8 μm pore size; Becton Dickinson), and the insert was placed in a 24-well dish containing starvation medium with or without 10% FBS[32,33]. When used, inhibitors were added to both chambers. Migration assays were performed for 4–6 h and cells were fixed with 3.7% formaldehyde. Cells were stained with crystal violet staining solution, and cells on the upper side of the insert were removed with a cotton swab. Three randomly selected fields (×10 objectives) on the lower side of the insert were photographed, and the migrated cells were counted. Migration was expressed as either the average number of migrated cells in a field or as a percentage of the migrated cells in the positive control. The percentage of migrated cells, P, was calculated with the formula $P = 100 \times (M - M_{nc})/M_{pc}$, where M is the number of migrated cells, M_{nc} is the number of migrated cells in negative controls, and M_{pc} is the number of migrated cells in positive controls.

Cell invasion assay. Cells (10^5) suspended in starvation medium were added to the upper chamber of a Matrigel-coated insert (6.5 mm diameter, 8 μm pore size; Becton Dickinson), and the insert was placed in a 24-well dish containing medium with or without serum. When used, inhibitors were added to both chambers. Invasion assays were performed for 16 h and cells were fixed with 3.7% formaldehyde. Cells were stained with crystal violet staining solution, and cells on the upper side of the insert were removed with a cotton swab. Three randomly selected fields (10× objectives) on the lower side of the insert were photographed, and the cells on the lower surface of the insert were counted.

Protein expression and purification. Recombinant GST–fascin fusion protein was produced in BL21 *Escherichia coli*. A 1-litre culture was grown to an attenuance at 600 nm (D_{600}) of 1.0 and then induced by the addition of 0.3 mM isopropyl β-D-thiogalactoside (IPTG) for 12 h at 25 °C. Cells were flash frozen and then lysed by sonication in Tris-buffered saline. The supernatant was then incubated with glutathione-Sepharose for 2 h at 4 °C. After extensive washing, GST–fascin was eluted and concentrated with a Centricon Plus-20 (Millipore). To remove the GST tag from the fusion protein, beads were incubated overnight at 4 °C with thrombin. The supernatant was collected and concentrated.

GST–fascin and biotin–macroketone interaction. Purified recombinant fascin protein or control protein were incubated with biotin–macroketone for 2 h at 4 °C. Proteins associated with biotin–macroketone were precipitated with Ultralink-immobilized Streptavidin-agarose (Pierce). After extensive washing, bound proteins were eluted with SDS sample buffer and resolved by 10% SDS–PAGE.

F-actin bundling assay. Actin-bundling activity was measured by low-speed centrifugation assay and fluorescence microscopy. In the low-speed centrifugation assay, monomeric rabbit G-actin was induced to polymerize at room temperature in F-actin buffer (20 mM Tris-HCl pH 8, 1 mM ATP, 1 mM dithiothreitol (DTT), 2 mM $MgCl_2$, 100 mM KCl). Recombinant fascin proteins or control buffer were subsequently incubated with F-actin for 60 min at room temperature and centrifuged for 30 min at 10,000*g* in an Eppendorf 5415D table-top centrifuge. Both supernatants and pellets were dissolved in an equivalent volume of SDS sample buffer, and the amount of actin was determined by SDS–PAGE. We measured the intensities of fascin proteins in Coomassie-stained gels and then calculated the relative actin-bundling activity, P, by the following formula: $P = 100 \times M_p/M_{pc}$, where M_p is the percentage of actin present in the pellet when mixed with different concentrations of fascin protein, calculated by (intensity in pellet)/(intensity in pellet + intensity in supernatant), and M_{pc} is the percentage of actin present in the pellet when mixed with 0.25 μM fascin, which is used at a saturated concentration determined in our control experiment.

In fluorescence microscopy, monomeric G-actin was polymerized as described earlier. F-actin was mixed with recombinant fascin protein in F-buffer (100 mM KCl, 2 mM $MgCl_2$, 1 mM ATP, 20 mM Tris-HCl pH 8.0) and incubated at room temperature for 30 min. Actin was then labelled by adding 5% rhodamine–phalloidin to the mixture. The samples were mounted between a slide and a coverslip coated with polylysine and imaged by fluorescence microscopy. Three randomly selected fields (×10 objectives) were photographed, and the bundles were counted. The number of bundles per field was expressed as the mean ± s.d.

Immunofluorescence microscopy. Cells cultured on gelatin-coated glass coverslips were fixed for 10 min at room temperature with 3.7% formaldehyde in PBS, permeabilized with 0.1% Triton X-100 for 5 min, and then washed three times with PBS. To block non-specific binding, the cells were incubated for 30 min with a solution of PBS containing 1% BSA and then incubated for 1 h with primary antibody at appropriate dilutions. After incubation with primary antibody, cells were washed three times with PBS and incubated with fluorescence-conjugated secondary antibody (Molecular Probes). The coverslips were then fixed onto slides and imaged with a Zeiss fluorescence microscope.

Electron microscopy. Samples were absorbed for 2 min onto freshly glow-discharged, carbon-coated copper grids and stained with 2% uranyl acetate. Grids were examined with a Zeiss electron microscope at an accelerating voltage of 80 kV.

4T1 breast tumour metastasis in mice. All animal work was performed in compliance with the guidelines of the Institutional Animal Care and Use Committee of the Weill Medical College. The spontaneous 4T1 mouse breast tumour metastasis assay was conducted as described previously[31,34]. Female BALB/c mice (6–8 weeks old) were purchased from the Jackson Laboratory. 4T1 tumour cells (10^5) were injected subcutaneously into the abdominal mammary gland area of mice by using 0.1 ml of a single-cell suspension in PBS on day 0. The dosage of tumour implantation was determined empirically to give rise to tumours about 10 mm in diameter in untreated wild-type mice within 21–23 days. Starting on day 7, when the tumours averaged about 4–5 mm in diameter, test compounds or control PBS saline were given every day by intraperitoneal injection at 10 mg kg^{-1} per mouse until day 25. On day 28, the mice were killed. This dosage regimen was well tolerated with no signs of overt toxicity. Each group included five mice. Primary tumours were measured with electronic calipers on the day that the mice were killed. Numbers of metastatic 4T1 cells in lungs were determined by the clonogenic assay. In brief, lungs were removed from each mouse on day 28, finely minced and digested for 2 h at 37 °C in 5 ml of enzyme cocktail containing PBS and 1 mg ml^{-1} collagenase type IV, on a platform rocker. After incubation, samples were filtered through 70-μm nylon cell strainers and washed twice with PBS. Resulting cells were suspended, plated with a series of dilutions in 10-cm tissue culture dishes in RPMI1640 medium containing 60 μM thioguanine for clonogenic growth. Because 4T1 tumour cells are resistant to 6-thioguanine, metastasized tumour cells formed foci after 14 days, at which time they were fixed with methanol and stained with 0.03% methylene blue for counting.

MDA-MB-231 human breast tumour lung colonization in mice. NOD-SCID immunodeficient mice were used for experimental lung colonization experiments. MDA-MB-231 human breast tumour cells expressing the TGL reporter were trypsinized and washed with PBS. This artificial TGL reporter gene encodes a triple fusion protein with herpes simplex virus 1 thymidine kinase fused to the N terminus of enhanced GFP and firefly luciferase fused to the C terminus of GFP[34,35]. Subsequently, 10^6 cells in 0.2 ml PBS were injected into the lateral tail vein. Luciferase-based, non-invasive bioluminescent imaging and analysis were performed with an IVIS Imaging System (Xenogen).

Microarray gene expression analysis. Gene expression data for fascin were extracted from each tumour sample and mean-centred across all samples for each. Tissues from primary breast cancers were obtained from therapeutic procedures performed as part of routine clinical management at Memorial Sloan-Kettering

Cancer Center (MSKCC). All research procedures with human tissue were approved by the MSKCC institutional review board[36]. Tissues were snap-frozen in liquid nitrogen and stored at −80 °C. Each sample was examined histologically with haematoxylin/eosin-stained cryostat sections. Regions were dissected manually from the frozen block to provide a consistent tumour cell content of more than 70% in tissues used for analysis. Total RNA was extracted from frozen tissue by homogenization in guanidinium isothiocyanate-based buffer (Trizol; Invitrogen), purified with RNAeasy (Qiagen) and examined for quality by denaturing agarose-gel electrophoresis. Complementary DNA was synthesized from RNA with a T7-promoter-tagged oligo(dT) primer. RNA target was synthesized from cDNA by *in vitro* transcription, and labelled with biotinylated nucleotides (Enzo Biochem). Gene expression analysis was performed with HG-U133A and U133B oligonucleotide microarrays in accordance with the manufacturer's instructions (Affymetrix). To identify differential gene expression, we used two different measures: fold change (ratio) between the normalized means of each group of samples, and a Student's *t*-test. The microarray data had previously been deposited at Gene Expression Omnibus (GEO) under accession number GSE2603.

Human fascin 1 expression and purification. Recombinant human fascin 1 was expressed as a GST fusion protein in *E. coli*. Typically, 1 litre of 2YT medium with antibiotic was inoculated overnight with 3 ml of BL21/DE3 culture transformed with pGEX4T-Fascin1 plasmid and grown at 37 °C until D_{600} reached about 0.8. The culture was then transferred to 22 °C and 0.1 mM IPTG was added for induction. After induction overnight, the bacteria were harvested by centrifugation at 5,000 r.p.m. for 10 min. The bacteria pellet was snap-frozen with liquid nitrogen and suspended in 30 ml of PBS supplemented with 0.2 mM PMSF, 1 mM DTT, 1% Triton X-100 and 1 mM EDTA. After sonication, the suspension was centrifuged at 15,000 r.p.m. for 60 min to remove the cell debris. The supernatant was then incubated for 2 h with 4 ml of glutathione beads (Sigma) at 4 °C. After extensive washing with PBS, the beads were resuspended in 10 ml of thrombin cleavage buffer (20 mM Tris-HCl pH 8.0, 150 mM NaCl, 2 mM $CaCl_2$, 1 mM DTT). Human fascin 1 was released from the beads by incubation overnight with 40–100 U of thrombin at 4 °C. After centrifugation, 0.2 mM PMSF was added to the supernatant to inactivate the remnant thrombin activity. The fascin protein was further purified with a Superdex 200 gel-filtration column and concentrated with Centricon to about 80 mg ml^{-1}. The typical yield from a 1-litre culture was about 40 mg.

Crystallization and structure determination. The concentrated protein stock solution was diluted with the protein buffer (20 mM Tris-HCl pH 8.0, 40 mM KBr, 0.5 mM EDTA, 1 mM DTT) to 15 mg ml^{-1} before crystallization. To obtain crystals of the fascin–macroketone complex, the protein was incubated for 1 h at room temperature in the protein buffer supplemented with 2 mM macroketone. Crystallization was performed at 20 °C with the vapour-diffusion hanging-drop method. Fascin crystallized in 100 mM HEPES pH 8.0, 16% PEG4000, 1% propan-2-ol. Both crystals (fascin without or with macroketone) belong to space group *C*2. Crystals were transferred briefly to the cryo-solution, which consisted of the crystallization solution supplemented with 15% glycerol, then flash-cooled in liquid nitrogen. X-ray diffraction data were recorded at National Synchrotron Light Source beamline X6A and X4C at Brookhaven National Laboratory. A partial structure was initially solved by the MR-SAD method with a selenomethionine derivative sample that diffracted to 2.1 Å and a fraction of the 1DFC PDB file. This model was subsequently extended by iterative model building and refinement cycles using COOT[37] and REFMAC5 (ref. 38). The fascin structure was solved by the molecular replacement method with the selenomethionine MR-SAD structure as a starting model and finally refined by following the same procedure. The diffraction of some fascin crystals was markedly improved by an 'annealing' process involving one freeze–thaw–freeze treatment. A 1.8 Å data set obtained from an annealed crystal rendered a markedly improved electronic density map, which was unambiguous throughout almost the entirety of both molecules in the asymmetric unit. The asymmetric unit contains two mostly complete molecules with the exception of four highly flexible loops (residues 1–7, 49–54 and 245–247 in chain A, and residues 1–7 and 300–303 in chain B) with poorly defined electron density. For the crystals of the complex of fascin and macroketone, one of the two molecules in the asymmetric unit is relatively disordered. An approximately 4σ peak was observed in the difference density map (Supplementary Fig. 7) near the surface of β-trefoil 4 of molecule A, on the side facing the cleft between trefoil 4 and trefoil 1. The ring structure was easily discernible in the difference map, and densities for the side chains were missing. The approximate orientation of the macroketone molecule was derived by fitting the macrolide ring into the density while keeping in mind the possible polar interactions between macroketone and fascin.

Statistical analysis. Data are expressed as means and s.d. and were analysed with Student's *t*-test; significance is defined as $P < 0.05$.

31. Shan, D. *et al.* Synthetic analogues of migrastatin that inhibit mammary tumor metastasis in mice. *Proc. Natl Acad. Sci. USA* **102,** 3772–3776 (2005).
32. Yang, S. & Huang, X. Y. Ca^{2+} influx through L-type Ca^{2+} channels controls the trailing tail contraction in growth factor-induced fibroblast cell migration. *J. Biol. Chem.* **280,** 27130–27137 (2005).
33. Shan, D. *et al.* The G protein $G\alpha_{13}$ is required for growth factor-induced cell migration. *Dev. Cell* **10,** 707–718 (2006).
34. Yang, S., Zhang, J. J. & Huang, X. Y. Orai1 and STIM1 are critical for breast tumor cell migration and metastasis. *Cancer Cell* **15,** 124–134 (2009).
35. Ponomarev, V. *et al.* A novel triple-modality reporter gene for whole-body fluorescent, bioluminescent, and nuclear noninvasive imaging. *Eur. J. Nucl. Med. Mol. Imaging* **31,** 740–751 (2004).
36. Doane, A. S. *et al.* An estrogen receptor-negative breast cancer subset characterized by a hormonally regulated transcriptional program and response to androgen. *Oncogene* **25,** 3994–4008 (2006).
37. Emsley, P. & Cowtan, K. Coot: model-building tools for molecular graphics. *Acta Crystallogr. D* **60,** 2126–2132 (2004).
38. Vagin, A. A. *et al.* REFMAC5 dictionary: organization of prior chemical knowledge and guidelines for its use. *Acta Crystallogr. D* **60,** 2184–2195 (2004).